Polariton propagation in shallow-confinement heterostructures: Microscopic theory and experiment showing the breakdown of the dead-layer concept

S. Schumacher, G. Czycholl, and F. Jahnke
Institute for Theoretical Physics, University of Bremen, D-28334 Bremen, Germany

I. Kudyk, H. I. Rückmann, and J. Gutowski
Institute for Solid State Physics, Semiconductor Optics Group, University of Bremen, D-28334 Bremen, Germany

A. Gust, G. Alexe, and D. Hommel
Institute for Solid State Physics, Semiconductor Epitaxy Group, University of Bremen, D-28334 Bremen, Germany
(Received 19 July 2004; revised manuscript received 20 September 2004; published 29 December 2004)

Polariton effects due to the interplay of the excitonic polarization of a semiconductor and a propagating light field are studied for transmission spectra of $ZnSe/ZnS_xSe_{1-x}$ heterostructures. Calculations in terms of microscopic boundary conditions for the exciton motion within a finite-height confinement potential can explain the measured transmission spectra. These calculations also show the absence of polarization-free regions near the sample interfaces. Macroscopic models based on Pekar's additional boundary conditions can only reproduce the spectra if the band alignment at the $ZnSe/ZnS_xSe_{1-x}$ interfaces is modified in comparison to the microscopic calculation and if a sample thickness is used that exceeds the independently determined experimental value. Our findings demonstrate the breakdown of the dead-layer concept for shallow confinement potentials.

DOI: 10.1103/PhysRevB.70.235340 PACS number(s): 71.36.+c, 71.35.Cc

I. INTRODUCTION

Since the introduction of the polariton concept[1] the proper description of a propagating light field interacting with the excitonic resonances of a semiconductor medium has been a long standing problem. For the idealized case of propagation within an infinitely extended semiconductor, the eigenmodes of the propagating light field coupled to the excitonic states can be easily formulated[2] since in this situation the exciton relative and center-of-mass motion are decoupled. Complications arise from the inclusion of sample surfaces where an external light field is coupled to the polariton modes and where the polaritons radiatively decay into photons.

In the past, macroscopic approaches have been introduced which continue using the excitonic susceptibility of the spatially homogeneous (infinitely extended) medium. In this case the inclusion of sample surfaces requires so-called additional boundary conditions (ABCs). The original proposal of Pekar[3] requires the vanishing of the macroscopic polarization at the semiconductor surface. Other approaches suggest that the spatial derivative[4] or a linear combination of the polarization and its derivative[5] should vanish at the sample surface. The missing microscopic foundation of ABCs for the coupled exciton and light field propagation in spatially inhomogeneous media has been the motivation for an alternative macroscopic formulation.[6]

Another effect that has to be included in macroscopic approaches is the reduced excitonic polarization near surfaces due to finite extension of the exciton relative motion. So-called dead-layers (leading to an effectively reduced sample thickness) have often been used in the past as a fit parameter. The determination of the dead-layer thickness based on a Born-Oppenheimer approximation has been discussed in Ref. 7.

Unfortunately the results for the excitonic transmission and reflection spectra in thin semiconductor layers strongly depend on the particular treatment of boundaries within the macroscopic models. These ambiguities can be avoided within a microscopic formulation of boundary conditions which are imposed on the solution of a two-particle Schrödinger equation for the electron-hole motion under the influence of Coulomb interaction which is directly coupled to Maxwell's equations for the propagating light field. A microscopic solution for this problem has been suggested in Ref. 8 for a semiconductor sample in half-space and slab geometry. The treatment of light reflection on a single surface within a half-space geometry has been presented in Ref. 9 using a contact potential for the Coulomb interaction. Recently the full solution of the linear light propagation problem has been applied to a finite semiconductor layer.[10] Only with microscopic boundary conditions was it possible to simultaneously reproduce amplitude and phase measurements of the transmitted light field through a GaAs layer.[10,11] Another investigation,[12] based on the approach of Ref. 8, has also demonstrated the critical role of microscopic boundary conditions for the half-space and slab geometry where again a one-dimensional contact interaction between the electrons and holes has been used.

Previous theoretical investigations have focused on infinitely high confinement potentials for the optically excited electrons and holes. In typical experiments, however, polariton propagation is studied in layers surrounded by buffer material. These heterostructures provide a confinement potential that is relatively high in the $GaAs/Al_{0.3}Ga_{0.7}As$ system of Refs. 10 and 11 but considerably shallower in the ZnCdSe/ZnSe system[13] or in ZnSe/ZnSSe structures.[14]

The purpose of this paper is to study polariton effects in ZnSe/ZnSSe as a model material system for shallow con-

finement within a direct comparison between transmission experiments and calculations using microscopic boundary conditions. As an alternative to the full numerical solution of the two-particle Schrödinger equation in Refs. 10 and 11 we use an expansion in terms of exciton wave functions for a layer with finite height of the carrier confinement potential.

Our approach deviates from Refs. 8 and 12 as we use exciton basis states computed for the confinement geometry, i.e., the semiconductor layer including finite-height potentials. In principle, the basis sets are equivalent, but in praxis a truncation is necessary. For the bulk basis used in Refs. 8 and 12, a large number of states is necessary to reach convergency of the wave function at the sample boundaries. On the contrary, in our approach each basis state fulfills the microscopic boundary conditions separately. Our new approach has several advantages. (i) In the linear case, different polariton resonances are uncoupled. Hence the number of basis states relates only to the number of included resonances, i.e., to the investigated spectral window. With different basis states different parts of the spectrum can be analyzed separately. (ii) Most of the numerical work is concentrated on the calculation of the basis states including microscopic boundary conditions. However, this calculation needs to be done only once for a given sample geometry. The calculations of the polariton spectra themselves are greatly simplified. (iii) Since the boundary conditions are fulfilled for every basis state, the accuracy of the wave functions is much higher. A suitable discretization of the wave function can easily be achieved.

Multiple reflections at the outer surfaces of the heterostructure are included in the solution of Maxwell's equations. We also show results for a macroscopic model based on Pekar's ABCs which is usually closer to the experiment and microscopic calculations in comparison to other macroscopic approaches. In the present case, the best fit of the Pekar model is obtained for an effective sample thickness that exceeds the true layer thickness which is independently determined using high-resolution x-ray diffraction. The microscopic calculations reveal this surprising result as an interplay between the extension of the exciton wave function into the shallow barriers and the reduction of the polarization near the barrier due to the finite extension of the exciton relative motion.

II. THEORY

We consider a semiconductor heterostructure consisting of a single ZnSe layer sandwiched between two ZnS_xSe_{1-x} layers as illustrated in Fig. 1. The structure homogeneously extends in the *x*-*y* plane and has a finite thickness in the *z* direction. Our calculations are based on a two-band model with spin-degenerate conduction and heavy-hole valence bands. This model is appropriate to describe the lowest interband transitions for the ZnSe layer with strain-split light- and heavy-hole valence bands for biaxial compressive strain (see the Appendix for more details). In order to obtain a lattice-matched structure to the GaAs substrate the sulfur content has to be less than 7%. An important property of these $ZnSe/ZnS_xSe_{1-x}$ heterostructures is the relatively small

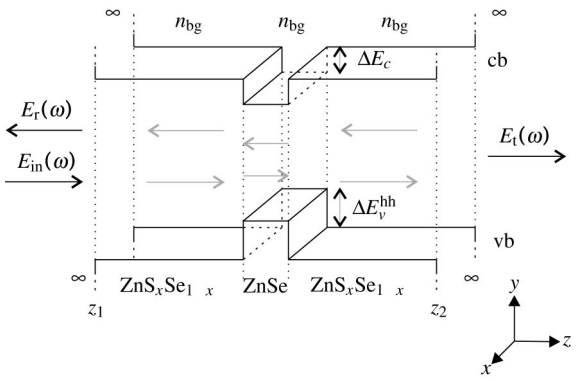

FIG. 1. Illustration of the considered semiconductor heterostructure in a slab geometry. Conduction band (cb) and heavy-hole valence band (vb) alignments are visualized. The system homogeneously extends in the *x*-*y* plane and has a finite thickness $|z_2-z_1|$ in the *z* direction. For more details see text.

height of the confinement potentials ΔE_c and ΔE_v^{hh} for the carrier motion in the *z* direction. The outer sample surfaces at z_1 and z_2 act as infinitely high potential barriers for electrons and holes.

For a circularly polarized transverse electromagnetic field propagating in the *z* direction we use the ansatz $\mathbf{E}(\mathbf{r},\omega)=E(z,\omega)\mathbf{e}_+$ and $\mathbf{B}(\mathbf{r},\omega)=B(z,\omega)i\mathbf{e}_+$ with $\mathbf{e}_+=1/\sqrt{2}(\mathbf{e}_x+i\mathbf{e}_y)$ in terms of the standard Cartesian basis vectors. Then in the semiconductor a macroscopic polarization of the form $\mathbf{P}(\mathbf{r},\omega)=P(z,\omega)\mathbf{e}_+$ is induced. We consider an incoming plane-wave light field with electric field amplitude $E_{in}(\omega)$ that is partly reflected at the semiconductor surface z_1 with an amplitude $E_r(\omega)$ and partly transmitted through the heterostructure with an amplitude $E_t(\omega)$. The nonresonant background refractive index n_{bg} inside the sample is assumed to be equal for ZnSe and ZnS_xSe_{1-x} in good approximation for the considered sulfur contents. In Sec. II A the microscopic theory to calculate the transmitted and reflected field amplitude is formulated. In Sec. II B we briefly summarize the phenomenological polariton theory based on Pekar's ABCs in the form used for the discussions in the following sections.

A. Microscopic theory

In the linear optical regime, the resonant contribution to the macroscopic polarization for electronic interband transitions can be given in the form[8]

$$P(z,\omega)=\int dz' E(z',\omega)\chi(z,z',\omega), \tag{1}$$

with the frequency dependent and nonlocal excitonic susceptibility

$$\chi(z,z',\omega)=-|d_{eh}|^2\sum_m\sum_{\mathbf{k},\mathbf{k}'}\frac{\phi_m^*(\mathbf{k}',z',z')\phi_m(\mathbf{k},z,z)}{\hbar\omega+i\gamma-\varepsilon_m}. \tag{2}$$

Here, $\mathbf{k}$ denotes the excitonic in-plane relative momentum, d_{eh} is the dipole matrix element between conduction and heavy-hole valence band, and γ a phenomenological dephas-

ing constant for the excitonic polarization. The exciton wave functions $\phi_m(\mathbf{k},z_e,z_h)$ enter the susceptiblity (2) only for equal electron and hole positions $z_e=z_h$ due to the use of a local dipole matrix element $d_{eh}(z_e-z_h)=d_{eh}\delta(z_e-z_h)$. The eigenenergies ε_m and wave functions $\phi_m(\mathbf{k},z,z')$ of the excitonic Hamiltonian

$$\mathcal{H}^X_{\mathbf{k},\mathbf{k}'}=(\varepsilon^e_{\mathbf{k},z_e}+\varepsilon^h_{\mathbf{k},z_h})\delta_{\mathbf{k},\mathbf{k}'}-V^{z_ez_h}_{\mathbf{k},\mathbf{k}'}, \tag{3}$$

are determined according to the following microscopic boundary conditions: The exciton wave functions vanish if either the electron or the hole reaches the semiconductor surface at z_1 or z_2. Note that these boundary conditions are fulfilled for each single exciton wave function $\phi_m(\mathbf{k},z_e,z_h)$ in contrast to previous formulations.[8,12] The one-particle energies in effective-mass approximation are

$$\varepsilon^i_{\mathbf{k},z_i}=\frac{\hbar^2k^2}{2m^*_{i\|}}-\frac{\hbar^2}{2m^*_{iz}}\frac{\partial^2}{\partial z_i^2}+\frac{E_{\mathrm{gap}}}{2}+V^i_{\mathrm{ext}}(z_i), \tag{4}$$

where $m^*_{e\|},m^*_{ez}$ and $m^*_{h\|},m^*_{hz}$ denote the effective electron and hole masses for in-plane ($\|$) and z direction, respectively. The external potential $V^i_{\mathrm{ext}}(z)$ is used to model the band offsets of the heterostructure. The Coulomb matrix elements are given by

$$V^{zz'}_{\mathbf{k},\mathbf{k}'}=\frac{e_0^2}{2\varepsilon_0 n_{\mathrm{bg}}^2}\frac{e^{-|\mathbf{k}-\mathbf{k}'||z-z'|}}{|\mathbf{k}-\mathbf{k}'|} \tag{5}$$

with $|\mathbf{k}-\mathbf{k}'|=\sqrt{k^2+k'^2-2kk'\cos(\phi_k-\phi_{k'})}$. Here e_0 is the absolute value of the electronic charge and ε_0 is the vacuum dielectric constant. In linear optics only excitons with in-plane s symmetry are optically excited. This is due to the rotational invariance of the system with respect to the z direction. An in-plane angular momentum decomposition yields the Hamiltonian projected to the in-plane s subspace.[15] The evaluation of the excitonic polarization in the excitonic eigenbasis turns out to be advantageous if only a few lowest excitonic states are optically excited. For our system, the considered states are well separated from the neglected part of the spectrum. Therefore a truncation of the excitonic basis represents a very good approximation in comparison to the full calculation.[10,11,15] The scalar wave equation for the electric field reads

$$\left[\frac{\partial^2}{\partial z^2}+n_{\mathrm{bg}}^2\frac{\omega^2}{c_0^2}\right]E(z,\omega)=-\frac{\omega^2}{\varepsilon_0c_0^2}\int dz'\chi(z,z',\omega)E(z',\omega). \tag{6}$$

Within the medium we use as an ansatz for the electric field coupled to the excitonic polarization

$$E_{\mathrm{med}}(z,\omega)=a(\omega)e^{iq(\omega)z}+b(\omega)e^{-iq(\omega)z}+\int dz'G(z,z',\omega)\times\left[-\frac{\omega^2}{\varepsilon_0c_0^2}\int dz''\chi(z',z'',\omega)E(z'',\omega)\right], \tag{7}$$

where $a(\omega)$ and $b(\omega)$ are the amplitudes of the free propagating and counterpropagating contributions solving the homogeneous part of Eq. (6). Treating the right-hand side of Eq. (6) as an inhomogeneity, its formal solution is found by adding a particular solution with the Green's function

$$G(z,z',\omega)=-\frac{i}{2q(\omega)}e^{iq(\omega)|z-z'|}. \tag{8}$$

The dispersion of the free solution is given by $q^2(\omega)=n_{\mathrm{bg}}^2(\omega^2/c_0^2)$ where c_0 is the vacuum velocity of light. The solution outside of the sample is given by the sum of the incoming and reflected plane wave for $z<z_1$ and a transmitted plane wave for $z>z_2$. The self-consistency requirement of the coupled light-matter interaction enters in our description of the spatially inhomogeneous system via the inhomogeneity in Eq. (6) depending on the solution itself. This approach yields a unique solution of the problem with respect to Maxwell's boundary conditions, namely, the continuity of the electric field $E(z,\omega)$ and its first derivative $(\partial/\partial z)E(z,\omega)$ at the sample boundaries for $z=z_1,z_2$.

B. Additional boundary conditions

In this section we summarize the application of a phenomenological polariton model to calculate optical transmission spectra for the above discussed heterostructure. To avoid the involved solution of the excitonic problem in the presence of an external potential on a microscopic level, the phenomenological model starts from the analytically known solution in a bulk crystal. In the absence of sample boundaries, a separation of the electron-hole relative and center-of-mass motion is possible. For the relative motion under the influence of Coulomb interaction and the free center-of-mass motion, the contribution of the 1s exciton can be described using the susceptibility

$$\chi(q,\omega)=\frac{|d_1|^2}{\hbar\omega+i\gamma-\varepsilon_1-\dfrac{\hbar^2q^2}{2M^*}}, \tag{9}$$

where ε_1 is the 1s exciton energy, M^* the total exciton mass, q the center-of-mass momentum, and $|d_1|^2=|d_{eh}|^2/(\pi a_0^{x3})$ is the dipole coupling of the 1s state to the electric field with the bulk exciton Bohr radius a_0^x. Taking into account propagating $E^+_{p=1,2}(\omega)$ and counterpropagating $E^-_{p=1,2}(\omega)$ contributions for the two resulting polariton modes $q_{p=1,2}(\omega)$ in the vicinity of the 1s exciton resonance, the ansatz for the electric field inside the layer is given by

$$E_{\mathrm{med}}(z,\omega)=\sum_{p=1,2}[E^+_p(\omega)e^{iq_p(\omega)z}+E^-_p(\omega)e^{-iq_p(\omega)z}]. \tag{10}$$

An essential property of this phenomenological approach is that Maxwell's boundary conditions at the sample surfaces and the ZnSe/ZnSSe interfaces are not sufficient to find a unique solution for the unknown field amplitudes. To overcome this fundamental shortcoming one imposes ABCs on the macroscopic polarization

$$P(\omega,z)=\sum_{p=1,2}\chi(q,\omega)|_{q=q_p(\omega)}\times[E^+_p(\omega)e^{iq_p(\omega)z}+E^-_p(\omega)e^{-iq_p(\omega)z}]. \tag{11}$$

The original ABCs of Pekar require a vanishing macroscopic

polarization at the boundaries of the layer that resonantly interacts with the light field.[3]

The advantage of this approach is simplicity. However, results may strongly depend on the used ABC scheme. Other models[4,6] are not considered here as Pekar's ABCs are most commonly used and yield best results in comparison to microscopic theory and experiment.[11]

It should be noted that the need for macroscopic ABCs results from the use of a local excitonic susceptibility, (9). The corresponding decoupling of the exciton relative and center-of-mass motion is clearly violated near the sample boundaries. To account for a finite spatial extension of the exciton, macroscopic ABCs have been augmented by the dead-layer assumption where an effectively reduced sample thickness due to polarization-free surface regions is considered. The dead-layer thickness should depend on the electron-hole mass ratio.[7,15] It is commonly used, however, as a fit parameter. This situation is additionally complicated by the fact that in many cases the sample thickness is not sufficiently well known. To remove this uncertainty for the samples used in this paper the thickness has been independently determined by means of high resolution x-ray diffraction, see Sec. III for details. Both the coupling of exciton relative and center-of-mass motion as well as the appearance of surface regions of reduced polarization are fully included in our microscopic solution of the two-particle problem for the electron-hole motion under the influence of Coulomb interaction and the external confinement potential.

III. SAMPLE GROWTH, CHARACTERIZATION AND OPTICAL SETUP

Three ZnSe/ZnSSe samples with nominal thicknesses of 20, 28, and 40 nm for the ZnSe layer were grown by molecular beam epitaxy (MBE) in a twin-chamber system on GaAs(001) substrates on which a 180-nm-thick GaAs buffer layer was deposited. The ZnSe layers are asymmetrically imbedded in ZnSSe lattice matched to the substrate with thickness of 1 μm (on the GaAs side) and 500 nm (on the top side).

The samples were characterized using a high resolution x-ray diffractometer with a Cu sealed anode, a four-crystal monochromator in Ge(220) configuration and a two-crystal analyzer. ω-2θ scans of the symmetrical (004) Bragg reflection show good lattice matching of the ZnSSe layers with respect to the substrate which allowed the coherent growth of the heterostructures. The resulting composition of the ZnSSe barriers as well as the thickness of the ZnSe layers extracted from calculated ω-2θ patterns are given in Table I. Reciprocal space maps of the asymmetrical (224) Bragg reflection confirmed that the structures are fully strained.

For transmission experiments the opaque GaAs substrate was removed by grinding and subsequent chemical etching. To measure the linear transmission spectra a conventional setup was used consisting of a Xe lamp with a filter transmitting the interesting blue spectral region only, a cryostat, a double-grating spectrometer with a spectral resolution of 10^{-4} eV, and a photomultiplier. All experiments were performed on free standing samples immersed in a liquid helium bath with a temperature of 4 K.

TABLE I. Structural sample parameters determined by high resolution x-ray diffraction and input parameters for the microscopic theory for the different samples. Band offsets are deduced from the structural data, see the Appendix. The layer thicknesses for the microscopic theory agree with the experimental ones, within an error of ±0.8 nm. For the macroscopic model the layer thicknesses are chosen so that the best fit is obtained for a reproduction of the experimental transmission spectra.

Nominal ZnSe layer thickness [nm]	20	28	40
Experimentally determined			
ZnSe layer thickness [nm]	21.5	29.0	43.5
Barrier sulfur content x [%]	5.2	5.0	5.8
Parameters for microscopic theory			
ZnSe layer thickness [nm]	20.7	29.4	43.7
Heavy-hole val. band offset ΔE_v^{hh} [meV]	21.2	20.6	23.2
Conduction band offset ΔE_c [meV]	2.7	2.1	4.6
Parameters for Pekar's ABCs			
ZnSe layer thickness [nm]	22.5	31.5	45.5

Free standing samples had to be used to avoid additional stress due to cooling down the samples. The chemical etching of the substrate had to be stopped in time to avoid an etching down of the ZnSSe-barrier on the bottom of the active layer. Therefore, the total thickness of the interesting transparent ZnSSe/ZnSe/ZnSSe system was checked after the etching process by an additional optical measurement. To do this, transmission spectra were measured over an extended spectral range to observe some periods of the Fabry-Perot modes which are due to the whole thickness of the system and are responsible for the absolute values of the transmission measured in the interesting spectral region of the hh-polariton modes. From comparison of the spectral behavior of the Fabry-Perot modes measured and calculated, the total thickness was obtained. For the samples used in the experiments it was in good agreement with the thickness previously intended in the MBE growth process. All samples show very pronounced polariton mode structures with distances depending on their active layer thickness.

IV. THEORY vs EXPERIMENT: RESULTS AND DISCUSSION

In this section we investigate the optical transmission spectra for the three samples described in Sec. III. The measured transmission spectra in the vicinity of the excitonic resonances of the ZnSe layer are shown as dashed lines in Fig. 2 for the (a) 20 nm, (b) 28 nm, and (c) 40 nm sample, respectively. Because of the high quality of the heterostructures even the weaker polariton resonances are clearly resolved. All peaks that can uniquely be attributed to resonances of the 1*s* heavy-hole polariton in the finite ZnSe layer are labeled with hh and consecutive numbers. While light-hole resonances are not considered in the calculations, at least the lowest light-hole (lh) resonance (and even higher resonances in the 40 nm layers) can be seen in the experi-

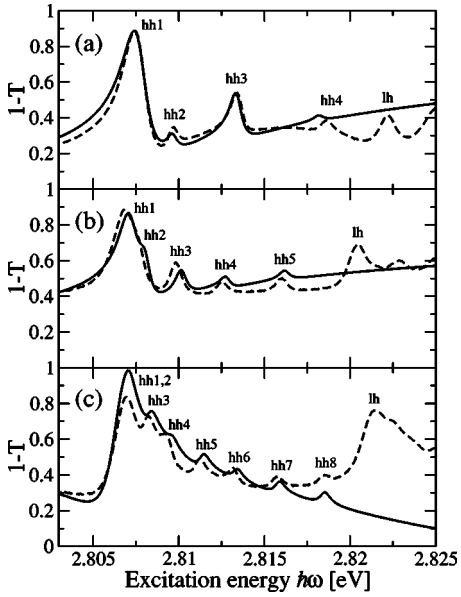

FIG. 2. Transmission spectra for the (a) 20 nm, (b) 28 nm, (c) 40 nm sample. Dashed line: Experiment. Solid line: Microscopic theory.

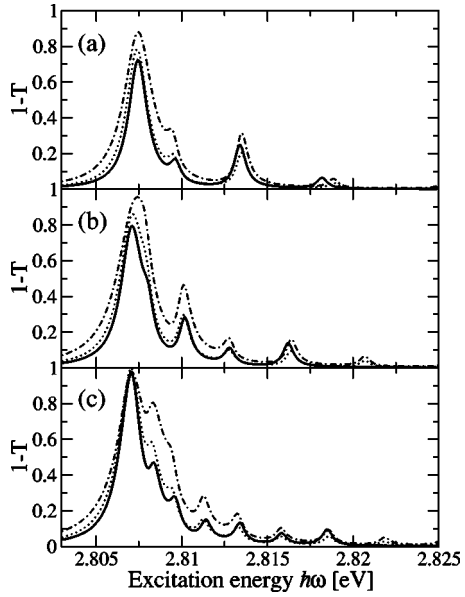

FIG. 3. Transmission spectra for the (a) 20 nm, (b) 28 nm, and (c) 40 nm sample without Fabry-Perot effects. Solid line: Microscopic theory, $d_{eh}/e_0=3.7$ Å. Dotted line: Pekar's ABCs, $d_{eh}/e_0=2.89$ Å. Dashed-dotted line: Pekar's ABCs, $d_{eh}/e_0=3.7$ Å.

ment. In each figure, the resulting spectrum from the microscopic theory is given by the solid lines. Input parameters are given in Tables I and II. In a good approximation to the experimental setup, a vacuum background refractive index $n_{\mathrm{bg}}=1$ is used outside the sample. The results demonstrate that the microscopic theory well reproduces the experimental findings for the considered part of the spectrum. The deviations for higher energies result from the not considered light-hole exciton contributions, higher heavy-hole exciton states, and the neglected frequency dependent dispersion of the ZnSSe layers in this frequency range. It should be noted that in the linear regime various polariton resonances are decoupled.[15] The dephasing constant γ and the band-gap energy $E_{\mathrm{gap}}(\mathrm{ZnSe})$ for the heavy-hole conduction band transition in the strained ZnSe layer (Table II) are adjusted according to the experimental values.

The surfaces of the heterostructure form a resonator for the optical field. The resulting Fabry-Perot modes are superimposed to the polariton resonances. To concentrate exclusively on the polariton effects in the ZnSe layer, the solid lines in Fig. 3 show results of the microscopic calculation

TABLE II. ZnSe material parameters for the microscopic theory, equal for all samples. For material parameters entering the macroscopic model see discussion in the text. The bare electron mass is denoted by m_0.

Gap energy	$E_{\mathrm{gap}}(\mathrm{ZnSe})=2.82593$ eV
Dephasing constant	$\gamma=0.35$ meV
Dipole coupling	$d_{eh}/e_0=3.7$ Å
Backgr. refractive index	$n_{\mathrm{bg}}=2.95$
Effective electron mass	$m_e^*=m_{e\parallel}^*=m_{ez}^*=0.147\ m_0$ (Ref. 16)
Luttinger parameter	$\gamma_1=2.45$ (Ref. 16)
Luttinger parameter	$\gamma_2=0.61$ (Ref. 16)

without Fabry-Perot effects (which corresponds to an ideal antireflection coating of the outer sample surfaces). For the macroscopic model, isotropic effective masses m_e^*, $m_{\mathrm{hh}}^*=m_{\mathrm{hhz}}^*$ for electrons and holes have to be used to facilitate the analytical solution, Eq. (9), which necessitates a slightly shifted band-gap energy $E_{\mathrm{gap}}^{\mathrm{Pekar}}=2.8289$ eV in comparison to the microscopic theory. The results are shown as dashed-dotted lines for a dipole coupling $d_{eh}/e_0=3.7$ Å and as dotted lines for $d_{eh}/e_0=2.89$ Å, respectively.

The dipole coupling $d_{eh}/e_0=3.7$ Å corresponds to the value of the microscopic theory. However, for the macroscopic model it turns out to be not appropriate. This is due to the assumption of homogeneity that enters the macroscopic model and that is not fulfilled for our system. For a meaningful comparison with the microscopic theory, an effectively reduced dipole coupling constant is extracted from the microscopic theory in the following way: Within a homogeneous system the reduced exciton mass μ^* is connected to the exciton binding energy $E_b^x(3D)$ by

$$\mu^* = \frac{32\pi^2\varepsilon_0^2 n_{\mathrm{bg}}^4 \hbar^2}{e_0^4} E_b^x(3D). \tag{12}$$

Using the exciton binding energy $E_b^x=19$ meV obtained from the microscopic theory for the anisotropic system, it is possible to extract an effective reduced exciton mass μ_{eff}^*. This yields an effective exciton Bohr radius

$$a_{0,\mathrm{eff}}^x = \frac{4\pi n_{\mathrm{bg}}^2 \varepsilon_0 \hbar^2}{\mu_{\mathrm{eff}}^* e_0^2}, \tag{13}$$

which, together with the dipole coupling constant $d_{eh}/e_0=3.7$ Å, provides an effective longitudinal-transversal splitting

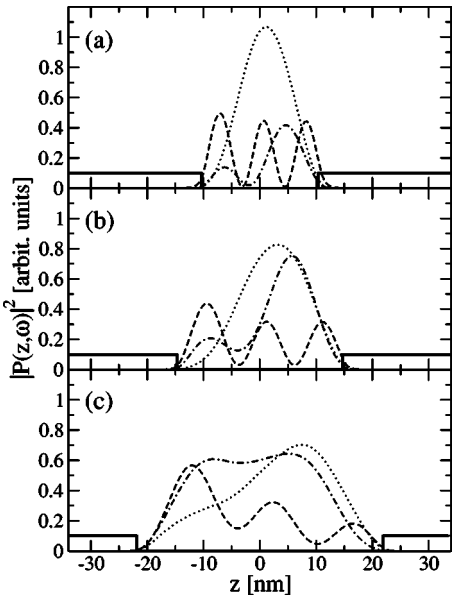

FIG. 4. Steady-state polarization for monochromatic, resonant excitation of the three lowest polariton modes in the microscopic theory without Fabry-Perot effects for the (a) 20 nm, (b) 28 nm, and (c) 40 nm sample. The excitation frequency is tuned to the first (dotted line), second (dashed-dotted line), or third (dashed line) resonance, respectively. The solid lines illustrate the confinement potential for carriers in the ZnSe layer.

$$\Delta_{\mathrm{LT}}^{\mathrm{mic}} = \frac{|d_{eh}|^2}{\pi n_{\mathrm{bg}}^2 \varepsilon_0 a_{0,\mathrm{eff}}^{x3}}. \tag{14}$$

With the assumption $\Delta_{\mathrm{LT}}^{\mathrm{Pekar}} = \Delta_{\mathrm{LT}}^{\mathrm{mic}}$ we obtain an effectively reduced dipole coupling constant $d_{eh}/e_0 = 2.89$ Å for the macroscopic model. Our discussion shows that within a macroscopic model for a homogeneous system applied to an inhomogeneous semiconductor heterostructure the dipole coupling constant is underestimated. In principle, the commonly used determination of dipole coupling constants from the longitudinal-transversal splitting is not appropriate here since Eq. (14) is only valid for homogeneous materials.

For each calculation based on Pekar's ABCs the layer thickness is adjusted for best reproduction of the energy positions of the polariton resonances in the experimental spectrum. The resulting values are given in Table I. The values for the layer thickness chosen for the macroscopic model are *even larger* than the values that are experimentally determined as well as used for the microscopic calculation. At first glance this is contradicted by the fact that for infinitely high potential barriers of the ZnSe layer there is a polarization-free region near the surface due to the finite extension of the exciton relative motion (which is often included as a dead-layer in macroscopic models).[7,11,15] Previous microscopic calculations for the $GaAs/Al_xGA_{1-x}As$ system clearly identified these polarization-free regions.

For a better understanding of these apparent inconsistencies in the application of Pekar's ABCs, Fig. 4 shows the spatially resolved macroscopic excitonic polarization obtained from the microscopic theory for resonant monochromatic excitation of the lowest three polariton states. Due to the relatively small height of the confinement potentials in the ZnSe/ZnSSe system, the exciton wave functions can even penetrate slightly into the barrier region. This shows that for shallow confinement potentials the "effective" sample thickness used in the macroscopic calculations based on ABCs can even exceed the true layer thickness, and that in this case the dead-layer concept breaks down.

It is interesting to note that in a layer with a high confinement potential the thickness of the region of reduced polarization varied for different polariton resonances of a given sample.[11] In the cases displayed in Fig. 4 this variation is much less pronounced. Especially for the 40 nm sample the effective thickness is almost the same for the displayed polariton modes. This also explains previous interpretations of experiments for ZnSe/ZnSSe heterostructures[14] in terms of Pekar's ABCs using the same effective thickness for all resonances of a given sample. As it turns out now, the used sample thickness exceeds the true value. However, the spatial dependence of the macroscopic polarization in Fig. 4 clearly deviates from a simple picture of quantization of the center-of-mass motion which shows the intricate interplay of relative and center-of-mass motion with the propagating light field.

V. CONCLUSION

A solution of the two-particle Schrödinger equation for the description of electron-hole-pair excitations under the influence of Coulomb interaction has been used to apply microscopic boundary conditions in a shallow confinement potential situation for which ZnSe/ZnSSe heterostructures served as a model example. Results for the polariton modes in transmission spectra reproduce the experimental observations while calculations based on Pekar's ABCs require unrealistic modifications of the material parameters. This is due to the fact that Pekar's ABCs assume an infinite-height confinement potential where the realistic inclusion of the exciton relative motion requires a polarization-free dead-layer. For shallow-confinement situations, a breakdown of these concepts has been demonstrated since the application of Pekar's ABCs requires an effective sample thickness which even exceeds the thickness of the confinement potential.

Generally the use of macroscopic ABC models inherits uncertainties in the used sample thickness to fit the spectral position and oscillatory strength of *all* polariton resonances of the same spectrum. In the studied examples of this paper, the counteracting influence of a shallow confinement potential, the band offset, and the carrier masses result in exciton wave functions having nearly the same effective extension. This is, however, by no means trivial and strongly dependent on the material system.

ACKNOWLEDGMENTS

We acknowledge a grant for CPU time from the John von Neumann Institute for Computing at the Forschungszentrum Jülich.

APPENDIX: MATERIAL PARAMETERS

This appendix is dedicated to the material parameters that are used to model the electronic band structure and its offsets

at the semiconductor interfaces. The effective masses for the heavy-hole valence band that follow from the Luttinger Hamiltonian in axial approximation are[17]

$$m^*_{\mathrm{hh}\|} = \frac{m_0}{\gamma_1 + \gamma_2} = 0.327 m_0, \tag{A1}$$

$$m^*_{\mathrm{hhz}} = \frac{m_0}{\gamma_1 - 2\gamma_2} = 0.813 m_0 \tag{A2}$$

for the in-plane motion and the motion in the growth direction, respectively. Different effective masses for the ZnSe and ZnSSe material are not considered because they would yield only minor changes to our results: Changes in the electron mass are negligible due to the small sulfur contents. The hole states contributing to the optical spectra only slightly penetrate the barrier due to the larger heavy-hole band offsets and the large effective heavy-hole mass. In good approximation, the optical band-gap bowing for a ternary compound is given by

$$E^{AB_xC_{1-x}}_{\mathrm{gap}} = (1-x)E^{AC}_{\mathrm{gap}} + xE^{AB}_{\mathrm{gap}} - bx(1-x). \tag{A3}$$

For the ZnSe/ZnSSe material system a variety of bowing parameters $b(\mathrm{ZnS}_x\mathrm{Se}_{1-x})$ has been reported.[18] We use an intermediate value of 0.43 eV, so that the literature values are accumulated around it. Gap energies of the pure binary bulk materials are[19]

$$E^{\mathrm{ZnS}}_{\mathrm{gap}}(T = 5\ \mathrm{K}) = 3.84\ \mathrm{eV}, \tag{A4}$$

$$E^{\mathrm{ZnSe}}_{\mathrm{gap}}(T = 5\ \mathrm{K}) = 2.82\ \mathrm{eV}. \tag{A5}$$

The ZnSe gap energy coincides quite well with the result for our samples (compare Table II and keep in mind its strain enlargement). For the unstrained bulk materials the valence band offset from ZnSe to ZnS is $\Delta E_v(\mathrm{ZnSe,ZnS}) = 530$ meV.[20] Similar results have been reported elsewhere.[21,22] With the gap energies this yields a conduction band offset of $\Delta E_c(\mathrm{ZnSe,ZnS}) = 490$ meV. We assume that the ratio of valence and conduction band offsets from pure ZnSe to $\mathrm{ZnS}_x\mathrm{Se}_{1-x}$ does not depend on the sulfur concentration x for the unstrained bulk materials. Due to pseudomorphic growth on GaAs(001) substrate, the ZnSe layer is biaxially compressively strained. This yields energy shifts of its conduction and valence bands.[23,24] The resulting energy shifts for conduction and heavy-hole valence band are given by[17]

$$\Delta E_{c,\mathrm{strain}} = 2a_c\left(1 - \frac{C_{12}}{C_{11}}\right)\varepsilon_{xx}, \tag{A6}$$

$$\Delta E^{\mathrm{hh}}_{v,\mathrm{strain}} = 2a_v\left(1 - \frac{C_{12}}{C_{11}}\right)\varepsilon_{xx} - b_v\left(1 + 2\frac{C_{12}}{C_{11}}\right)\varepsilon_{xx}. \tag{A7}$$

Only a hydrostatic deformation potential is obtained for the conduction band whereas an additional shear deformation potential applies for the valence band shift. The hydrostatic deformation potential decreases the band offsets for both bands and thus enlarges the gap energy of the ZnSe material. The shear deformation potential increases the offset for the heavy-hole valence band and thus decreases the gap energy. The required material parameters for ZnSe are[21,24] $a_c = -5.9$ eV, $a_v = -1.0$ eV, $b_v = -1.14$ eV for the deformation potential constants and $C_{11} = 929$ kbar, $C_{12} = 562$ kbar for the elastic stiffness tensor elements. The strain tensor element $\varepsilon_{xx} = (a_{\|,\mathrm{ZnSe}} - a^0_{\mathrm{ZnSe}})/(a^0_{\mathrm{ZnSe}})$ follows from the in-plane lattice constants of the fully strained ($a_{\|,\mathrm{ZnSe}} = a_{\mathrm{GaAs}}$) and unstrained ($a^0_{\mathrm{ZnSe}}$) ZnSe material. The band offsets for the different samples follow from the sulfur concentration in Table I. They slightly vary around carrier confinement potentials of 3 meV for the conduction band and 22 meV for the heavy-hole valence band, compare Table I. The small conduction band offset coincides with previous results for ZnSe/ZnSSe heterostructures with larger sulfur concentrations.[23,25]

[1] J. J. Hopfield, Phys. Rev. **112**, 1555 (1958).

[2] H. Haug and S. W. Koch, *Quantum Theory of the Optical and Electronic Properties of Semiconductors*, 3rd ed. (World Scientific Publishing, Singapore, 1995).

[3] S. I. Pekar, Sov. Phys. JETP **6**, 785 (1958).

[4] C. S. Ting, M. J. Frankel, and J. L. Birman, Solid State Commun. **17**, 1285 (1975).

[5] V. A. Kiselev, B. S. Razbirin, and I. N. Uraltsev, Phys. Status Solidi B **72**, 161 (1975).

[6] K. Henneberger, Phys. Rev. Lett. **80**, 2889 (1998).

[7] M. Combescot, R. Combescot, and B. Roulet, Eur. Phys. J. B **23**, 139 (2001).

[8] A. D'Andrea and R. Del Sole, Phys. Rev. B **25**, 3714 (1982); A. D'Andrea and R. Del Sole, *ibid.* **41**, 1413 (1990).

[9] K. Victor, V. M. Axt, and A. Stahl, Z. Phys. B: Condens. Matter **92**, 35 (1993).

[10] J. Tignon, T. Hasche, D. S. Chemla, H. C. Schneider, F. Jahnke, and S. W. Koch, Phys. Rev. Lett. **84**, 3382 (2000).

[11] H. C. Schneider, F. Jahnke, S. W. Koch, J. Tignon, T. Hasche, and D. S. Chemla, Phys. Rev. B **63**, 045202 (2001).

[12] E. A. Muljarov and R. Zimmermann, Phys. Rev. B **66**, 235319 (2002).

[13] S. Lankes, M. Meier, T. Reisinger, and W. Gebhardt, J. Appl. Phys. **80**, 4049 (1996).

[14] U. Neukirch, K. Wundke, J. Gutowski, and D. Hommel, Phys. Status Solidi B **196**, 473 (1996).

[15] S. Schumacher, G. Czycholl, and F. Jahnke, Phys. Status Solidi B **234**, 172 (2002).

[16] H. W. Hölscher, A. Nöthe, and C. Uihlein, Phys. Rev. B **31**, 2379 (1985).

[17] S. L. Chuang, *Physics of Optoelectronic Devices, Wiley Series in Pure and Applied Optics* (Wiley-Interscience publication, New York, 1995).

[18] J. E. Bernard and A. Zunger, Phys. Rev. B **36**, 3199 (1987).

[19] K. Shahzad, D. J. Olego, and C. G. Van de Walle, Phys. Rev. B **38**, 1417 (1988).

[20] S.-H. Wei and A. Zunger, Appl. Phys. Lett. **72**, 2011 (1998).
[21] G. F. Schötz, W. Sedlmeier, M. Lindner, and W. Gebhardt, J. Phys.: Condens. Matter **7**, 795 (1995).
[22] C. G. Van de Walle and J. Neugebauer, Nature (London) **423**, 626 (2003).
[23] S. Lankes, B. Hahn, C. Meier, F. Hierl, M. Kastner, A. Rosenauer, and W. Gebhardt, Phys. Status Solidi A **152**, 123 (1995).
[24] B. Rockwell, H. R. Chandrasekhar, M. Chandrasekhar, A. K. Ramdas, M. Kobayashi, and R. L. Gunshor, Phys. Rev. B **44**, 11 307 (1991).
[25] S. Lankes, T. Reisinger, B. Hahn, C. Meier, M. Meier, and W. Gebhardt, J. Cryst. Growth **159**, 480 (1996).